Influence of defects and charges on the colloidalstabilization of graphene in water

Joao Paulo Vita Damesceno, Emmanuel Picheau, Ferdinand Hof, Aldo José Gorgatti Zarbin, Alain Penicaud, Carlos Drummond

Chemistry–A European Journal
Research Article
doi.org/10.1002/chem.202303508
Chemistry Europe
European Chemical Societies Publishing
www.chemeurj.org

Influence of Defects and Charges on the Colloidal Stabilization of Graphene in Water

João Paulo Vita Damasceno,[a, b] Emmanuel Picheau,[b] Ferdinand Hof,[b] Aldo J. G. Zarbin,[a] Alain Pénicaud,*[b] and Carlos Drummond*[b]

Mastering graphene preparation is an essential step to its integration into practical applications. For large-scale purposes, full graphite exfoliation appears as a suitable route for graphene production. However, it requires overpowering attractive van der Waals forces demanding large energy input, with the risk of introducing defects in the material. This difficulty can be overcome by using graphite intercalation compounds (GICs) as starting material. The greater inter-sheet separation in GICs (compared with graphite) allows the gentler exfoliation of soluble graphenide (reduced graphene) flakes. A solvent exchange strategy, accompanied by the oxidation of graphenide to graphene, can be implemented to produce stable aqueous graphene dispersions (Eau de graphene, EdG), which can be readily incorporated into many processes or materials. In this work, we prove that electrostatic forces are responsible for the stability of fully exfoliated graphene in water, and explore the influence of the oxidation and solvent exchange procedures on the quality and stability of EdG. We show that the amount of defects in graphene is limited if graphenide oxidation is carried out before exposing the material to water, and that gas removal of water before the incorporation of pre-oxidized graphene is advantageous for the long-term stability of EdG.

Introduction

Top-down methods for the production of graphene dispersions are commonly based on controlled graphite exfoliation and subsequent stabilization of the exfoliated material in a convenient solvent. For this purpose, two pathways have been proposed. 'Physical' methods put forward mechanical shearing (e.g. high-power sonication or ball-milling) of graphite, to overpower the van der Waals (vdW) forces that keep graphite layers together.[1] These low-cost processes are usually carried out in a liquid environment. They are easily scalable but have several drawbacks: first, large energy input promotes the appearance of defects and limits the production of large flakes, which can be detrimental for some applications; second, complete exfoliation (to single-layer graphene, SLG) is rarely achieved. In addition, stabilizing agents (e.g. surfactants or polymers) are required to prevent subsequent re-aggregation of the exfoliated material. These agents can have unwanted consequences on the final material such as decreased conductivity, for example. A second, "chemical" method is the well-known graphite oxide route where graphite is first oxidized, exfoliated, and dispersed as (insulating) graphene oxide (GO) in water.[2] After processing, GO must be reduced by thermal or chemical means to restore some conductivity. This method is efficient in terms of exfoliation and stabilization of graphene sheets but introduces many defects like holes and oxygen functional groups.

We, and others, have suggested a gentler chemical method for graphite exfoliation, based on the use of graphite intercalation compounds (GICs).[3,4,5,6–8] GICs are produced by inserting different chemical species between graphite layers.[9] The increased interplanar separation in the GICs and the charge transfer between graphite (host) and intercalant (guest) substitute the interlayer vdW interactions by electrostatic interactions between graphene sheets and intercalant layers that have opposite charges. It has been demonstrated that electron transfer between donor intercalants and graphite layers is the source of the solubility of these materials in polar solvents, making it possible for spontaneous, complete graphite exfoliation down to charged monolayers[3,4,5] After dissolution is achieved, SLG can be produced by suitable discharging of the graphenide (C_n^{m-}) polyanions.[5]

To avoid re-aggregation of (neutral) graphene, the addition of stabilizers is commonly required. It is remarkable, though, that aqueous graphene dispersions produced starting from potassium GIC after dissolution in THF and transfer to water (Eau de Graphene, EdG) are stable against flocculation or restacking for months, without the need for additives.[10] Destabilizing vdW attractive forces between thin flakes are significantly reduced (compared with 3D objects of similar size)

[a] Dr. J. P. Vita Damasceno, Prof. Dr. A. J. G. Zarbin
Department of Chemistry, Federal University of Paraná (UFPR), CP 19032, CEP 81531-980 Curitiba, PR, Brazil

[b] Dr. J. P. Vita Damasceno, Dr. E. Picheau, Dr. F. Hof, Dr. A. Pénicaud, Dr. C. Drummond
Centre de Recherche Paul Pascal (CRPP) UMR 5031-CNRS/Université de Bordeaux, 115 Av. Du Dr. Albert Schweitzer, 33600 Pessac, France
and
present address: Department of Analytical Chemistry, Institute of Chemistry, University of Campinas, P.O. Box 6154, 13084-971 Campinas, Brazil
E-mail: alain.penicaud@crpp.cnrs.fr
carlos.drummond@crpp.cnrs.fr

by virtue of their two-dimensional nature. At the simplest level, one can consider that the dispersive interaction between the graphene atoms is pairwise additive. Under this assumption, the van der Waals interaction energy per unit area E_{vdW}/A between thin flakes of thickness b, decays with the fourth power of the separation distance, D, as $E_{vdW}/A \approx \frac{A_{Ham}\cdot b^2}{2\cdot\pi\cdot D^4}$, for separation larger than the thickness (A_{Ham} is the suitable Hamaker constant).[11] In contrast, the interaction energy between spheres of radius R decays with the inverse of the separation distance, like $E_{vdW} \approx \frac{A_{Ham}\cdot R}{12\cdot\pi\cdot D}$, extending to a significantly longer distance range.[11] This dimensional reasoning is valid for fully exfoliated graphene in EdG, the ultimate thinnest limit, where graphene sheets have been separated from each other during the intercalation step. On the contrary, "graphene" dispersions obtained by sonicating graphite in the presence of a stabilizing agent always present a distribution of thicknesses, leading to stronger vdW attractive interactions. In any event, a stabilizing force is required to counterbalance the attractive interactions (despite their strength), to assure the stability of graphene dispersions. We have hypothesized that the stability of the dispersed graphene flakes in EdG is promoted by repulsive electrostatic interactions, which dominate over vdW and hydrophobic attractive forces.[10]

A key step in the preparation of charge-stabilized EdG is the re-oxidation method, which involves air exposure and transfer to water of the graphenide solutions.[10] Here, we compare different preparation methods of EdG, varying these steps and analysing the consequences in terms of defect formation and EdG stability. We found that defects are detrimental to stability, with important consequences: i) pristine graphene sheets are better stabilized by charges than defective ones, and ii) higher EdG concentration can be reached with lower defect concentration.

Results

The formation and colloidal stabilization of 'Eau de graphene'

Four different samples of EdG have been prepared, varying the re-oxidation conditions of the graphenide solutions (Scheme 1). The originally reported procedure for EdG production[10] includes the preparation of a KC_8 graphite intercalation compound,[12] its dissolution in THF, exposure of this graphenide solution (*vide infra*) to air, transfer to degassed water, and finally THF evaporation (see scheme 1 and experimental part). In order to test the influence of each step, the air exposure of the graphenide solution and the degassing of water were performed or not, leading to a 2×2 matrix of 4 samples (scheme 1): Sample a was oxidized then transferred to degassed water (original procedure);[10] sample b was not oxidized before transfer to degassed water; sample c was not oxidized before transfer to non-degassed water and sample d was oxidized before transfer to non-degassed water (Scheme 1). The Raman spectrum of sample a, corresponding to the original procedure, was collected directly from the liquid dispersion and obtained after subtraction of the water signal. It shows three bands characteristics of graphitic material: D, G, and 2D bands (Figure 1). The 2D band has a symmetrical shape, characteristic of non-interacting layers or single graphene layers.[13,14] Furthermore, its intensity is high, roughly twice that of the G band, as expected for a single graphene sheet.[15] This 2D band differs drastically from that of surfactant-based dispersions of (multilayer) graphene obtained by sonication, where the 2D band is of lower intensity than the G band and exhibits a composite shape due to interaction between AB stacked layers.[15] A D band can also be observed in the Raman spectrum (Figure 1). As we have shown in a previous work,[10] the intensity of the D band corresponds to a concentration of defects ca. 600 ppm.[16] These defects are the consequence of the exposition of graphenide to oxygen and moisture,[17] as will be discussed below. Finally, it can be observed in the photographs in the inset of Figure 1 that light is strongly scattered when a laser beam is shined through EdG (Tyndall effect), confirming the presence of submicron-size graphene particles dispersed in water.

In our original work,[10] it was proposed that the electrostatic repulsion between charged graphene sheets was responsible for the significant (meta)stability of EdG. To validate the likelihood of this hypothesis, we tested the response of the system to the addition of increasing amounts of $MgCl_2$. A one-month-old sample (a) was tested against the addition of

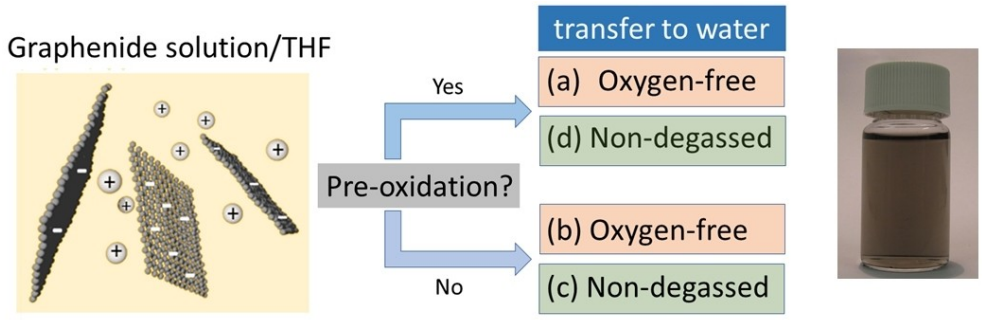

Scheme 1. Sample preparation: Graphite is intercalated with potassium to yield the KC_8 graphite intercalation compound (GIC) (not shown). KC_8 is then dissolved in THF to yield a graphenide solution (left image). The latter is oxidized (exposed to air) and added to oxygen-free water (sample (a)) or water naturally containing air (sample (d)). Alternatively, the graphenide solution is not oxidized and is directly added to oxygen-free water (sample (b)) or air-equilibrated water (sample (c)).

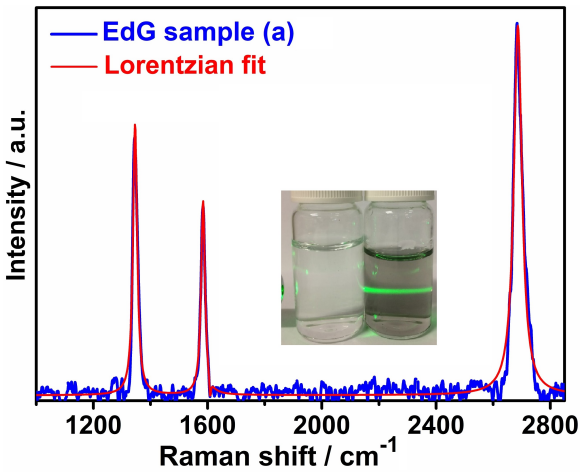

Figure 1. Raman spectrum (blue) of the sample (a) after subtraction of water signal. Lorentzian fit of the spectrum (red). Inset: Tyndall effect: the laser beam is visible due to light scattering by submicron-size particles in the sample (a) whereas it is invisible when it goes through a vial filled with pure water. Positions/linewidths of the bands are 1346/17.5 (D), 1584/16.6 (G), and 2687/34.5 cm^{-1} (2D).

increasing amounts of $MgCl_2$. We found that above an $MgCl_2$ threshold concentration of ca. 5 mmol L^{-1}, flocculation occurs (Figure 2A). The predictable destabilization is the consequence of the more substantial screening of the inter-flake electrostatic repulsion with increasing the ionic strength of the environment. At the critical coagulation concentration (CCC) of $MgCl_2$ (ca. 5 mmol L^{-1}) the attractive interflake interaction surpasses the electrostatic repulsion and fast aggregation and precipitation of graphene are observed. The UV-visible absorption spectrum of pure EdG (top blue spectrum in Figure 2B) shows the signature of neutral graphene at 269 nm, due to the π-π transition of the aromatic structure. Upon the addition of increasing amounts of $MgCl_2$, the intensity of the band at 269 nm decreases progressively due to graphene precipitation. At $MgCl_2$ concentrations above the CCC, graphene concentration is largely diminished (red spectrum and subsequent spectra).

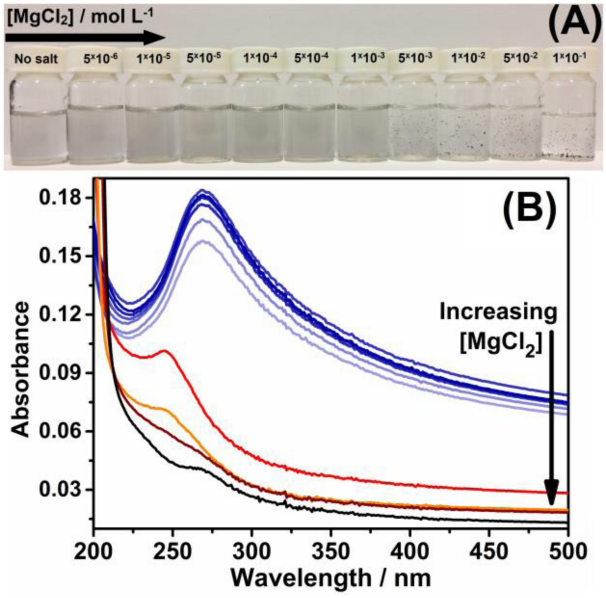

Figure 2. (A) Vials filled with a one-month-old sample (a) and increasing concentration of $MgCl_2$ from left to right. EdG dispersions are stable up to 1 mmol L^{-1} of $MgCl_2$, whereas above a threshold concentration of 5 mmol L^{-1}, flocculation, and precipitation occur. (B) UV-vis spectra of the 11 samples. The top spectrum corresponds to the outer left sample (no $MgCl_2$ added) whereas the bottom spectra corresponds to the outer right vial with 0.1 mmol L^{-1} $MgCl_2$. Up to 1 mmol L^{-1}, the UV-vis spectra decrease marginally in intensity but remain practically unchanged. For $MgCl_2$ concentrations of 5 mmol $L^{-1}$and above, the π-π absorption peak at 269 nm is lost and the absorbance nearly vanishes.

Destabilization along time and effects of the oxidation step on the colloidal stability

Several properties of the four samples (a) to (d) have been explored as a function of ageing time. Absorption spectra recorded weekly for 6 weeks are plotted in Figure 3. Two features are readily visible: i) the presence of a second band at 225 nm for samples (a), (b), and (c) and its disappearance after 3 weeks for all samples, and ii) large differences in the intensity of the 269 nm band between the samples, indicating significant disparity in graphene concentration since the first week. We have measured by gravimetry the mass concentration of dispersed material (30 to 40 mL each, dried in an oven at 100 °C). Samples (a) to (d) have concentrations next to 260, 100, 125, and 235 mg L^{-1}, respectively, just after THF evaporation. The band at 225 nm has been documented[18] as a signature of oxygenated defects on graphene oxide. Alternatively, superoxide ion O_2^-, or rather its hydrogenated form HO_2 also has an absorption band at 225 nm.[19] Graphenide oxidation by air bubbling leads to the formation of superoxide ions in a first step.[20] However, its lifetime is rather low[18] and it is highly improbable that it would last for several weeks. The presence of this 225 nm band in samples (a), (b), and (c) shows that defects have been generated during the preparation of EdG. It is noteworthy that sample (d) does not present any band at this wavelength. Nevertheless, in all cases this band disappears after 3 weeks of ageing, showing that these defects are detrimental to stability and that weakly oxygenated graphene sheets have eventually precipitated.

Regardless of the preparation route, all the EdG samples investigated presented a "clean" spectrum after 3-weeks of ageing: no sign of defective band at 225 nm and only absorption at 269 nm due to the π-π transition. It is noteworthy that the proportion of graphene in all samples improves with ageing, strongly suggesting the preferential precipitation of functionalized (non-pristine graphene) material. This 'self-cleansing' trait may prove of great interest for application purposes. Nevertheless, there are significant differences in graphene concentration between the different samples that translate into differences in absorbance. In particular, a significantly larger concentration of graphene was obtained when the graphenide solutions were oxidized before contact with water (samples (a) and (d)), even though the amount of graphenide per unit volume of water in the preparation of the

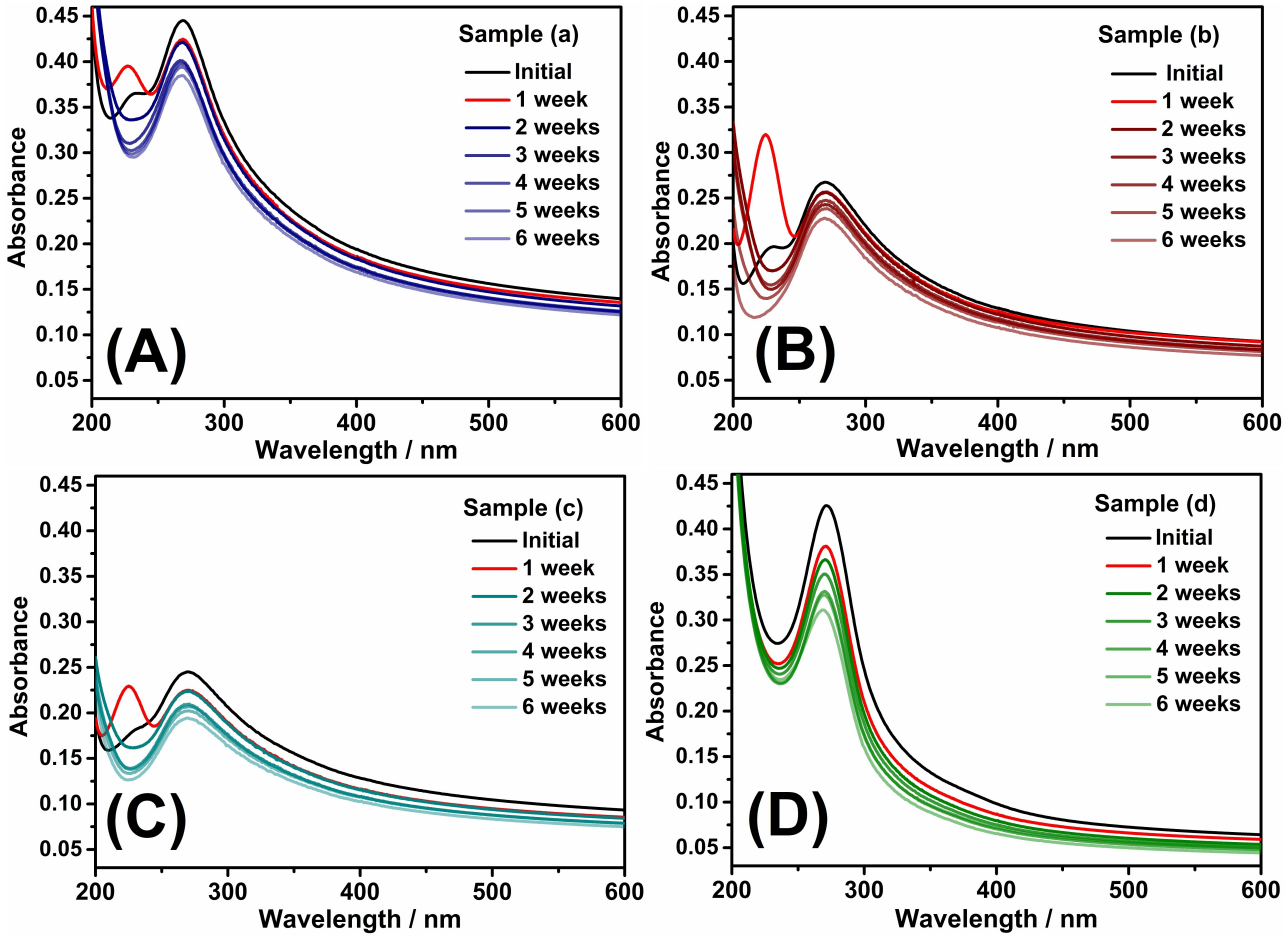

Figure 3. Time-dependent absorption spectra of samples (a) to (d). The initial time is defined as the end of THF evaporation, i.e. 3 days after mixing graphenide solutions and water. Samples (a) and (d) (graphenide solution oxidized before addition to water) are more concentrated than samples (b) and (c) (no prior oxidation before addition to water). Other than sample (d) (prior oxidation and addition to water naturally containing air), an absorption band at 225 nm is initially observed. In all cases, only the π-π-signal at 269 nm is observed after 3 weeks of ageing. This peak is reduced at 86% of its initial height in sample (a), 85% in sample (b), 79% in sample (c), and 73% in sample (d) after ageing for 6 weeks.

four samples was strictly identical. These aspects will be further discussed below.

Raman spectroscopy has proven to be a sensitive and versatile tool to characterize the properties of graphene-based materials with several characteristic bands observed, as discussed above. The G band is characteristic of sp^2 carbon whereas the D band is related to defect (local loss of symmetry).[21] Hence, the ratio of peak area between D and G bands, A_D/A_G, allows us to qualitatively and quantitatively compare the amount of defects between different samples. Figure 4 shows the frequency distribution of A_D/A_G for the four samples investigated in this work. We evaluated separately the Raman spectra of samples dried out of the different dispersions (drop casting). In the inset, the A_D/A_G distributions for the dried dispersion and the precipitate for the four samples are compared, both collected 3 weeks after THF evaporation. Sample (a) shows a similar maximum for both dispersion and precipitate, with a larger tailing towards high values for the latter. On the contrary, the three other samples show a higher A_D/A_G value for the maximum and a larger tailing towards high values for the precipitate. Thus, the four samples show a larger amount of defects for the precipitate than for the dispersion, with sample (a) showing the least difference and sample (d) the largest. In agreement with the UV-Vis observations, more defective/functionalized material appears to be less dispersible and more prone to precipitate.

Figure 5 shows a scanning electron microscope picture of a film prepared from fresh sample (a). The film was prepared by mixing EdG sample (a) with a mixture of water and toluene and letting the film self-organize at the liquid-liquid interface.[22,23] The film is homogeneous, presenting a wide variation of flake size, roughly centred around half a micron, and shows the quality of films prepared from EdG.

Discussion

Several effects deserve discussion regarding the results, namely (i) stabilization of the EdG dispersions by charges, (ii) defect formation and identification, and (iii) stability vs charges, time, and defect concentration.

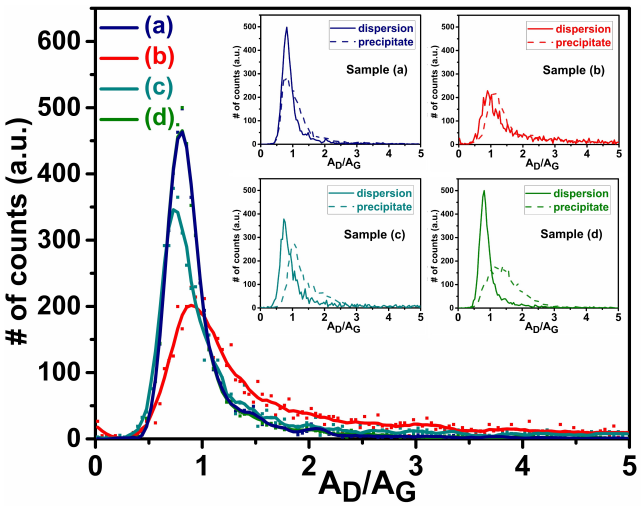

Figure 4. Frequency distribution of the area ratio A_D/A_G for material from the four dispersions after drying (3 weeks-old dispersions). Samples (a) and (d), in which graphenide was oxidized before contact with water, have virtually indistinguishable A_D/A_G distribution. They are the narrowest with the lowest tail towards high A_D/A_G. Sample (b) has the largest tail towards high A_D/A_G ratios pointing to a larger amount of defects. Inset: A_D/A_G frequency distribution for the dried solution *vs* its precipitate after three weeks of ageing for the four samples. All four precipitates show larger tailing towards high A_D/A_G ratios.

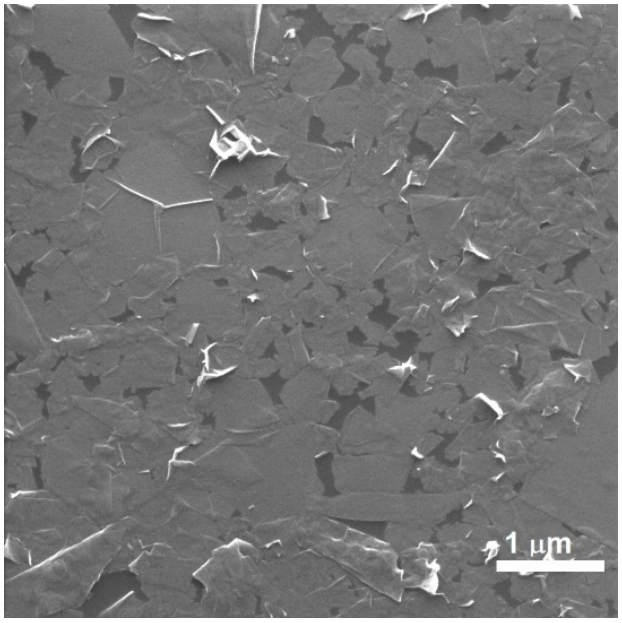

Figure 5. Scanning Electron Microscopy image of a film prepared from fresh sample (a) by the liquid/liquid interface method developed by some of us.[22,23]

EdG stability: repulsive electrostatic interaction

The results depicted in Figure 2, showing the abrupt destabilization of EdG above a certain ionic strength, demonstrate that repulsive electrostatic interactions are responsible for the remarkable stability of colloidal graphene in water, as hypothesized in our previous studies.[10] Indeed, significant electrophoretic mobility of graphene in water (pointing to negatively charged objects) has been observed by us and other groups.[24,25] As we have described before,[10] graphene stability is further assisted by the quickly decaying attractive vdW interactions with interflake distance, due to their 2D character.

Defect formation and identification

Defect formation on nanotubides or graphenides upon air exposure is a complex issue, which has been debated over the years and is still not fully settled. Some reports have shown full reversibility of the reduction (electron gain) followed by oxidation (electron loss),[26,27] whereas others have shown the irreversible formation of defect-like functional groups.[17,28]

Before discussing defects, one needs to be able to identify them. The UV-Vis absorption band at 225 nm (Figure 3) may be attributed to surface oxygenated functional groups, such as C–OH or epoxide groups.[18] Additionally, the increase of D band intensity vs that of G band in the Raman spectrum has long been recognized as the signature of an increase in defect concentration provided the graphenic units are larger than ca. 2 nm.[29,30,21]

As prepared, EdG shows in three cases (samples a, b, and c) the presence of a rather intense absorption band at 225 nm (Figure 3), sample (b) showing the highest intensity, and sample (d) having no signal at that wavelength. Samples (b) and (d) have opposite preparation protocols (Scheme 1). Sample (b) was not air-exposed before injection into the water; hence, the graphenide (electron-rich graphene) solution was directly injected into degassed, oxygen-free water. The electron-rich graphene was thus exposed to water but not oxygen, at any moment. This sample appears to have the largest concentration of oxygenated defects, likely -OH and others, coming from water (Figure 3). Likewise, statistical analysis of the Raman spectra of the dried dispersion (b) shows the highest tailing towards high A_D/A_G ratio (Figure 4), confirming that this sample has the highest concentration of defects. Conversely, sample (d) was air-exposed before being injected into non-degassed (*i.e.* oxygen-saturated) water. Thus, sample (d) was the most exposed to oxygen and presented the smallest amount of defects (no band at 225 nm in Figure 3 and the A_D/A_G distribution with the smallest tailing towards high values in Figure 4).

A hypothesis to explain these data is that graphenide exposed to oxygen undergoes preferentially a redox process, giving its extra electrons to oxygen leading to less charged graphene and superoxide $O_2^{\cdot-}$. Conversely, graphenide non-exposed to air (non-oxidized) reacts with water to produce functional groups such as C-OH or C–H.[17] A consequence of this is that if a graphenide solution has been sufficiently exposed to oxygen before injection into the water, it should not matter if the water is degassed or not (oxygen-free or not), regarding the amount of defects. Following this reasoning, let us analyse the other two samples, (a) and (c). Sample (a) was oxidized before injection into oxygen-free water and sample (c) was not oxidized before injection into oxygen-containing water.

Thus, sample (a) should have lost part of its extra electrons before exposure to water and should present a smaller amount of defects than sample (c). This is indeed observed in Figure 3: the intensity of the 225 nm peak compared to the π-π-absorption at 269 nm is lower for (a) than (c). Likewise, Figure 4 shows that sample (a) has a virtually indistinguishable A_D/A_G distribution from that of sample (d), i.e. the smallest signature for defects.

An important point, discussed in the results section, is that the 225 nm absorption band disappears after three weeks, suggesting some "self-cleaning" of the EdG. A hypothesis to explain this fact is that defects are not homogeneously distributed but that some graphene flakes are more defective than others. This could be if defects are preferentially at the edges. Then small fragments (larger edge proportion) will be more defective than larger ones. Indeed, a recent study has shown that graphene functionalization occurs within the vicinity of the edges, rendering smaller graphene homogeneously functionalized whereas larger ones are mostly functionalized in the vicinity of their periphery (not only at the edges), leaving their central zone free of functionalization.[31]

It is beyond the scope of this article to discuss if exposure of graphenide to oxygen promotes an electron exchange between graphenide and dioxygen only or preferentially. However, one can safely infer from our results that oxygen exposure of graphenide favours electron transfer at the expense of functionalization.

Concentration and stability

Stability issues are best analysed in Figure 3, where the π-π-signature at 269 nm indicates dispersed graphene sheets in water. At t0, *i.e.* after evaporation of THF, samples (a) and (d) show by far the highest concentration. Both have undergone air oxidation before addition to water and have the least defective material (*vide supra*). As an identical proportion of graphenide *vs* water was used to prepare the different samples, the difference in graphene concentration between the different samples points to a more significant material precipitation in the absence of graphenide pre-oxidation (samples (b) and (c)). This strongly suggests that the presence of defects is detrimental to graphene dispersibility in water. Furthermore, after 3 weeks of ageing, the small amount of precipitated material was separated from their respective dispersions. One can see in Figure 3 that dispersions no longer show the band at 225 nm: most defective material has precipitated away. Dried dispersions and precipitates were analysed statistically by Raman spectroscopy (Figure 4). The inset of Figure 4 compares, for the four samples, the dispersions and precipitates. In all cases, the precipitate is more defective (higher tailing of the A_D/A_G ratio towards high values) than the respective dried dispersion. At this point, we can only conjecture about the reasons for this unexpected and potentially useful 'self-cleaning' ability of the graphene dispersions investigated. It suggests that either the attractive vdW and hydrophobic interaction is stronger or the stabilizing negative charge is reduced for the case of functionalized species (or both). Regarding the attractive interaction, it appears that increasing functionalization, which presumably reduces the hydrophobicity of the material, enhances inter-particle attraction. Besides the hypothesis of preferential functionalization in the vicinity of the edges, we may speculate that increasing the proportion of structural defects favours folding and crumpling of the material, enhancing the long-range attractive vdW inter-particle interaction since 3D objects 'see' each other farther away than 2-D objects.[32]

Finally, comes the question of degassing, i.e. removal of gas including oxygen, from water. Two effects might play a role here: i) degassing removes oxygen from water, i.e. increases defect formation (*vide supra)*, hence should decrease both concentration and stability. However, these effects are probably minor if graphenide has been thoroughly oxidized before mixing with water. ii) Experimental evidences of gas nucleation on graphene/water[33,34] and graphite/water interfaces[35,36] have been reported. Degassing removes gases that might adsorb at the interface between graphene and water, hindering nanobubble nucleation and long-range capillary interactions and limiting aggregation.[37,38,39] In the absence of adsorbed gases attractive hydrophobic interaction may still act between the graphene flakes, but with a significantly shorter range of action.[40,39] There is some controversy regarding graphene-water wettability, although it is getting increasingly clear that, in virtue of its atomic thickness, the description of graphene surface energy must involve the media on both sides of the material (e.g. chemical nature of supporting substrate or fluid environment).[41] In this regard, it has been advanced that the interaction between graphene and water is favoured when it is wetted on each side because graphene acts as a 'translucent' medium which does not completely screen the van der Waals forces between water molecules on both sides.[42,43] Absence of gas adsorption should also allow ionic adsorption on graphene, hence enhancing the electrostatic charge and increasing the stability of the dispersion. Overall, degassing should help stability, especially if graphenide has been oxidized before.

In Scheme 1, water has been degassed in (a) and not in (d), the rest being equal. Likewise, water degassing has been done for (b) and not for (c) the rest being equal. After 6 weeks, sample (a) has lost 14% of its initial absorption whereas sample (d) has lost 27%. Likewise, sample (b) has lost 17% of its initial absorption whereas sample (c) has lost 27%. In both cases, degassing appears to have limited the loss of dispersed material with time, i.e. degassing helps stabilize graphene aqueous dispersions. This effect should be enhanced if caution is taken to minimize gas re-dissolution during storage.

Conclusions

With graphene applications on the rise, top-down graphene production from graphite is crucial. Obtaining individualized graphene sheets in liquids avoiding the highly defective GO

route as well as the size-shrinking surfactant and sonication route is possible via the dissolution of intercalation compounds, followed by the removal of electrons and transfer to water.[10] We have shown in this report that charges are responsible for the (meta)stability of graphene dispersions in water. Furthermore, defects appear to be detrimental to stability. The number of defects can be limited by full air oxidation of graphenide solutions before transfer to water. Finally, water degassing appears to have a double opposite role: removing oxygen leads to more defects if graphenide has not been exhaustively oxidized before. On the other hand, the absence of gas in water helps long-term stabilization of EdG. Another perspective is that regarding defects in the graphenide route, oxygen, and water, often considered as a global reactive medium, should be analysed separately. We conclude here that oxygen preferentially removes electrons from graphenides whereas water will preferentially lead to defects.

Experimental Section

Materials

Crystalline flake graphite with carbon content >99% and ash content less than 0.1% was obtained from Asbury Carbons (grade 3763, lot 12874); metallic potassium (98%), and magnesium chloride (>98%) from Sigma-Aldrich, and tetrahydrofuran (THF) from Carlo Erba (≥99.9%, HLPC non-stabilized). THF was purified through a Pure Solv 400-4-MD solvent purification system (Inert Corporation) connected to a glove box (Model: S1-DL, Inert Corporation), equipped with an air and moisture purifier and H_2O and O_2 sensors. The purified THF was distilled over NaK alloy inside the glove box. Deionized water was collected using a Millipore equipment, model Elix 10, and its resistivity was better than 18.2 MΩ.

KC_8 preparation and dissolution in THF

GICs preparation and dissolution were both performed in a glove box filled with argon, with oxygen concentration lower than 1 ppm. KC_8 was prepared by mixing graphite with molten potassium according to a previously published procedure.[12] Briefly, 106 mg of metallic potassium and 261 mg of graphite were added into a 20 mL glass vial and the mixture was heated in a hot plate at 180 °C. This mixture was stirred with a stainless-steel spatula until the solid material changed from shiny grey to golden colour. The solid was stirred every 15 min in the first hour, and then every hour during 4 h. The golden colour of KC_8 appears a few minutes after the heating started, so the initial stirring is the most critical for the homogeneity of the material. KC_8 dissolution was performed according to a previously published procedure.[10,12] Briefly, 100 mL of anhydrous THF were poured over 500 mg of recently prepared KC_8 (5 mg mL^{-1}) in a 150 mL Erlenmeyer, and the mixture was stirred at 130 rpm for 5 days with a glass-covered stirring bar (45 mm×8 mm).[44] After this period, the mixture was centrifuged at 2800 rpm for 20 min and the supernatant was transferred to 20 mL glass vials. The graphenide solution obtained was pale yellow.

Preparation of aqueous graphene dispersion, Eau de graphene

Sample (a) (pre-oxidized graphene in oxygen-free water) was prepared according to the procedure reported before.[10] Deionized water was degassed using a vacuum pump for 20 min and mild stirring with a PTFE bar to induce bubble nucleation. Graphenide solution was removed from the glove box inside glass vials just after centrifugation and bubbled with air for 5 seconds using a glass Pasteur pipette. The contact with oxygen turns the graphenide solution from yellow to dark grey due to the removal of electrons. The freshly oxidized graphenide solution was transferred to degassed water inside another glass vial. In each 20 mL glass vial, 3.75 g of oxidized graphenide solution and 15 g of degassed water (1:4 proportion of graphenide solution to water in mass) were mixed, and the vials containing the mixtures were left open inside a fume hood for 3 days to evaporate THF.

Sample (b) (no prior oxidation, oxygen-free water), was prepared as sample a, removing the step of oxidation by bubbling air and substituting the degassing of water by argon purging, then degassing. Graphenide solution (rather than re-oxidized graphenide solution) was thus directly transferred to water. To do so, graphenide solution was added to a glass syringe inside the glove box and used to wash the syringe three times (5 mL each time). Then, the syringe was filled with graphenide solution (25 mL, equivalent to 22 g) removed from the glove box, and transferred to oxygen-free water. In this case, water (88 g) was bubbled with argon for 15 min inside a closed round-bottom glass flask (rubber caps to allow needle insertion), degassed for 15 min and the pressure was increased again using argon. The non-oxidized graphenide solution inside the syringe (22 g) was added to the oxygen-free water (88 g), and then the round flask was opened to the atmosphere and left open for 3 days to evaporate THF.

Sample (c) (no prior oxidation and non-degassed water) was prepared as sample (b), removing the step of Ar purging and then degassing the water. Sample (d) (pre-oxidized graphene in non-degassed water) was prepared as sample (a) removing the step of degassing water.

For all samples, at the end of the preparation of EdG after THF evaporation, some minor precipitation has been observed. The supernatant was separated from the precipitated material.

Homocoagulation experiments of sample (a) with aqueous solutions of electrolytes

2.7 mL of one-month-old sample (a) and 2.7 mL of deionized water or $MgCl_2$ aqueous solution with different concentrations: 1×10^{-5}, 2×10^{-5}, 1×10^{-4}, 2×10^{-4}, 1×10^{-3}, 2×10^{-3}, 1×10^{-2}, 2×10^{-2}, 1×10^{-1} and 2×10^{-1} mol L^{-1} were mixed in 6 mL glass vials. The values of the final concentrations of electrolyte were half of the initial. The mixtures were shaken by hand and kept at rest for 48 h. After this period, pictures were taken, and the samples were analysed.

Thin film preparation at a liquid-liquid interface

In a 50 mL round-bottom glass flask, 20 mL of deionized water and 20 mL of toluene were added and the mixture was stirred at 1500 rpm. Sample (a) (10 mL, freshly prepared just after THF evaporation) was added to the biphasic liquid mixture under stirring, which was maintained for 24 h. After this period, the stirring was turned off and the phase separation was observed, along with material adsorption at the liquid-liquid interface as a thin, semitransparent film. This mixture was transferred to a 50 mL beaker containing the substrates on an L-shaped rod: (i) about

20 mL of the bottom phase (water) and 15 mL of the upper phase (toluene) were transferred to the beaker containing the substrates to be coated (silicon wafers and glass) using a glass pipette; (ii) the remaining mixture inside the round flask was stirred by hand and was poured at once into the beaker. After transfer, most of the upper liquid phase inside the beaker (toluene) was removed with a glass pipette (about 19 mL) and discarded, then the rod with the substrates was moved vertically and slowly to deposit the solid material adsorbed at the liquid-liquid interface. The substrates with thin film were dried inside a fume hood for 30 min and in an oven at 100 °C.

Sample characterization

UV-Vis spectroscopy was performed in a Jasco spectrometer, model V-730, from 200 to 900 nm. Aqueous samples were analysed using quartz cuvettes with 10 mm optical path, and transmittance blanks were recorded with the respective solvent.

Raman spectra were acquired with an Xplora Raman spectrometer (Horiba Jobin Yvon), using a green laser (2.33 eV; 532 nm), and a 1200 lines/mm grating. Frequency calibration was done using the HOPG peak at 1582 cm^{-1}. Solid samples were deposited over silicon substrates and analysed in mapping mode (200 μm×200 μm). Analysed spots were separated by 2.5 μm. The spectra were integrated 1 s, using 0.13 mW laser power, and a 50× objective lens. Liquid samples were analysed using a holder coupled to a macro objective of 20× and 10 mm quartz cuvette, performing 20 s of integration and 100 accumulations for each sample, and using 1.3 mW of laser power. The water spectrum was recorded in the same conditions and subtracted from the dispersion spectra.

Scanning electron microscopy (SEM) was performed in a Tescan microscope, model MIRA3 FEG-SEM, operating at 10 kV and using 5 mm of working distance. Images of secondary electrons were detected in the mode In-beam, close to the incident beam. Dispersed or solid samples were deposited over silicon substrates and dried at room temperature before analysis, and electrical contact was made using copper conductive tape.

Acknowledgements

A. J. G. Z. and A. P. thank CAPES/COFECUB for grant Ph–C931/19, J. P. V .D. thanks CAPES for a (CAPES-Print) fellowship, A. J. G. Z. and J. P. V. D. thank CNPq, INCT-Nanocarbon and INCT-NanoVida for financial support. F. H. thanks CNRS for a momentum grant; C. D. and A. P. thank l'Agence Nationale de la Recherche, project 2D-MEMBA, ANR-21-CE09-0034-01.

Conflict of Interests

The authors declare no conflict of interest.

Data Availability Statement

The data that support the findings of this study are available from the corresponding author upon reasonable request.

Keywords: graphene · graphene-based dispersions · graphite intercalation compounds · graphene Raman spectroscopy · dispersion stability of graphene

[1] D. W. Johnson, B. P. Dobson, K. S. Coleman, *Curr. Opin. Colloid Interface Sci.* **2015**, *20*, 367–382.
[2] S. Park, R. S. Ruoff, *Nat. Nanotechnol.* **2009**, *4*, 217–224.
[3] C. Vallés, C. Drummond, H. Saadaoui, C. a. Furtado, M. He, O. Roubeau, L. Ortolani, M. Monthioux, A. Pénicaud, *J. Am. Chem. Soc.* **2008**, *130*, 15802–15804.
[4] A. Catheline, C. Vallés, C. Drummond, L. Ortolani, V. Morandi, M. Marcaccio, M. Iurlo, F. Paolucci, A. Pénicaud, *Chem. Commun.* **2011**, *47*, 5470–5472.
[5] A. Pénicaud, C. Drummond, *Acc. Chem. Res.* **2013**, *46*, 129–137.
[6] J. Kwon, S. H. Lee, K.-H. Park, D.-H. Seo, J. Lee, B.-S. Kong, K. Kang, S. Jeon, *Small* **2011**, *7*, 864–868.
[7] E. M. Milner, N. T. Skipper, C. A. Howard, M. S. P. P. Shaffer, D. J. Buckley, K. A. Rahnejat, P. L. Cullen, R. K. Heenan, P. Lindner, R. Schweins, *J. Am. Chem. Soc.* **2012**, *134*, 8302–8305.
[8] E. Widenkvist, D. W. Boukhvalov, S. Rubino, S. Akhtar, J. Lu, R. A. Quinlan, M. I. Katsnelson, K. Leifer, H. Grennberg, U. Jansson, *J. Phys. D* **2009**, *42*, DOI 10.1088/0022-3727/42/11/112003.
[9] M. S. Dresselhaus, G. Dresselhaus, *Adv. Phys.* **1981**, *30*, 139–326.
[10] G. Bepete, E. Anglaret, L. Ortolani, V. Morandi, K. Huang, A. Pénicaud, C. Drummond, *Nat. Chem.* **2017**, *9*, 347–352.
[11] V. A. Parsegian, *Van Der Waals Forces A Handbook for Biologists, Chemists, Engineers, and Physicists*, Cambridge University Press, New York, **2005**.
[12] G. Bepete, F. Hof, K. Huang, K. Kampioti, E. Anglaret, C. Drummond, A. Pénicaud, *Phys. Status Solidi RRL* **2016**, *10*, 895–899.
[13] G. Bepete, A. Pénicaud, C. Drummond, E. Anglaret, *J. Phys. Chem. C* **2016**, *120*, 28204–28214.
[14] A. C. Ferrari, D. M. Basko, *Nat. Nanotechnol.* **2013**, *8*, 235–46.
[15] A. C. Ferrari, J. C. Meyer, V. Scardaci, C. Casiraghi, M. Lazzeri, F. Mauri, S. Piscanec, D. Jiang, K. S. Novoselov, S. Roth, A. K. Geim, *Phys. Rev. Lett.* **2006**, *97*, 187401.
[16] L. G. Cançado, A. Jorio, E. H. M. Ferreira, F. Stavale, C. A. Achete, R. B. Capaz, M. V. O. Moutinho, A. Lombardo, T. S. Kulmala, A. C. Ferrari, *Nano Lett.* **2011**, *11*, 3190–3196.
[17] F. Hof, S. Bosch, S. Eigler, F. Hauke, A. Hirsch, *J. Am. Chem. Soc.* **2013**, *135*, 18385–18395.
[18] Z. Zhang, H. C. Schniepp, D. H. Adamson, *Carbon* **2019**, *154*, 510–521.
[19] J. Stinchcombe, A. Penicaud, P. Bhyrappa, P. D. W. Boyd, C. A. Reed, *J. Am. Chem. Soc.* **1993**, *115*, 5212–5217.
[20] R. Ma, G. Lin, Y. Zhou, Q. Liu, T. Zhang, G. Shan, M. Yang, J. Wang, *npj Comput. Mater.* **2019**, *5*, 78.
[21] R. Beams, L. Gustavo Cançado, L. Novotny, *J. Phys. Condens. Matter* **2015**, *27*, 083002.
[22] V. H. R. Souza, S. Husmann, E. G. C. Neiva, F. S. Lisboa, L. C. Lopes, R. V. Salvatierra, A. J. G. Zarbin, *Electrochim. Acta* **2016**, *197*, 200–209.
[23] A. J. G. Zarbin, *Mater. Horiz.* **2021**, *8*, 1409–1432.
[24] K. B. Ricardo, A. Sendecki, H. Liu, *Chem. Commun.* **2014**, *50*, 2751–2754.
[25] M. M. Gudarzi, *Langmuir* **2016**, *32*, 5058–5068.
[26] A. Pénicaud, F. Dragin, G. Pécastaings, M. He, E. Anglaret, *Carbon* **2014**, *67*, 360–367.
[27] G. Bepete, N. Izard, F. Torres-Canas, A. Derré, A. Sbardelotto, E. Anglaret, A. Pénicaud, C. Drummond, *ACS Nano* **2018**, *12*, 8606–8615.
[28] A. Catheline, F. Paolucci, G. Valenti, P. Poulin, A. Pénicaud, *J. Mater. Res.* **2015**, *30*, 2009–2017.
[29] F. Tuinstra, J. L. Koenig, *J. Chem. Phys.* **1970**, *53*, 1126–1130.
[30] P. Mallet-Ladeira, P. Puech, C. Toulouse, M. Cazayous, N. Ratel-Ramond, P. Weisbecker, G. L. Vignoles, M. Monthioux, *Carbon* **2014**, *80*, 629–639.
[31] N. Rubio, H. Au, G. O. Coulter, L. Guetaz, G. Gebel, C. Mattevi, M. S. P. Shaffer, *Chem. Sci.* **2021**, *12*, 14907–14919.
[32] J. N. J. N. Israelachvili, *Intermolecular and Surface Forces*, Academic Press, **2011**.
[33] L. Zhou, L. Islas, N. Taylor, O. Bikondoa, E. Robles, W. H. Briscoe, *Carbon* **2019**, *143*, 97–105.
[34] X. Wang, B. Zhao, W. Ma, Y. Wang, X. Gao, R. Tai, X. Zhou, L. Zhang, *ChemPhysChem* **2015**, *16*, 1003–1007.

[35] B. M. Borkent, S. de Beer, F. Mugele, D. Lohse, *Langmuir* **2010**, *26*, 260–268.
[36] P. Janda, O. Frank, Z. Bastl, M. Klementová, H. Tarábková, L. Kavan, *Nanotechnology* **2010**, *21*, 095707.
[37] N. Ishida, M. Sakamoto, M. Miyahara, K. Higashitani, *Langmuir* **2000**, *16*, 5681–5687.
[38] P. Attard, *Adv. Colloid Interface Sci.* **2003**, *104*, 75–91.
[39] R. F. Tabor, C. Wu, F. Grieser, R. R. Dagastine, D. Y. C. Chan, *J. Phys. Chem. Lett.* **2013**, *4*, 3872–3877.
[40] H. Stevens, R. F. Considine, C. J. Drummond, R. A. Hayes, P. Attard, *Langmuir* **2005**, *21*, 6399–405.
[41] L. A. Belyaeva, G. F. Schneider, *Surf. Sci. Rep.* **2020**, *75(2)*, 100482, DOI 10.1016/j.surfrep.2020.100482.
[42] N. Ojaghlou, D. Bratko, M. Salanne, M. Shafiei, A. Luzar, *ACS Nano* **2020**, *14*, 7987–7998.
[43] J. Driskill, D. Vanzo, D. Bratko, A. Luzar, *J. Chem. Phys.* **2014**, *141*, 18C517.
[44] M. J. Kayatin, V. A. Davis, *J. Polym. Sci. Part A* **2013**, *51*, 3716–3725.

Manuscript received: October 25, 2023
Accepted manuscript online: February 18, 2024
Version of record online: ■■, ■■

RESEARCH ARTICLE

Graphite intercalation compounds allow gentle exfoliation of soluble graphenide (reduced graphene) flakes. Oxidation of graphenide to graphene and solvent exchange produce aqueous graphene dispersions (Eau de graphene, EdG), stabilized by electrostatic forces, with a minimal amount of defects if graphenide oxidation is carried out before exposure to water.

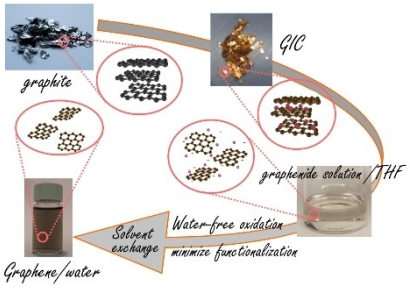

Dr. J. P. Vita Damasceno, Dr. E. Picheau, Dr. F. Hof, Prof. Dr. A. J. G. Zarbin, Dr. A. Pénicaud, Dr. C. Drummond**

1 – 10

Influence of Defects and Charges on the Colloidal Stabilization of Graphene in Water